© Strojniški vestnik 47(2001)8,403-410
ISSN 0039-2480
UDK 536.2
Izvirni znanstveni članek (1.01)

© Journal of Mechanical Engineering 47(2001)8,403-410
ISSN 0039-2480
UDC 536.2
Original scientific paper (1.01)

THE 3D SIMULATION OF THERMOMECHANICAL PROCESSES IN THE INDUSTRIAL PUSHER-TYPE FURNACE

Zdeněk Veselý
Department of Physics
University of West Bohemia
Univerzitní 22
Plzeň, CZ - 306 14
Czech Republic

Milan Honner
Mechanical Engineering Research
ŠKODA VÝZKUM s.r.o.
Tylova 57
Plzeň, CZ - 306 00
Czech Republic

ABSTRACT

The aim of the contribution is to present the current computational capabilities and results of thermomechanical processes simulation in the industrial furnace. Three-dimensional model of the continuous pusher-type furnace employed in mild rolling mill has been created. The resultant velocity and temperature distributions inside the furnace, heat flux and coefficient of heat transfer to the charge surface have been the important results used to support the development of the optimization control system for the furnace.

1. INTRODUCTION

Continuous industrial furnaces are used in steelworks to reheat slabs or billets before rolling. Such a furnace is usually divided into several regulated zones with several controlled gas-fired burners. The continuous heating process characterizes the mentioned kind of furnaces. Cold billets enter the furnace at one side and on the opposite side there is the output of hot billets. Pusher-type furnaces transport the billets in the furnace through the heating zone at the rate at which a new billets enter. Loading a new billet causes the oldest billet to be pushed out of the furnace at the other end. Walking beam furnaces transport the billets forward by a cyclic sequence of vertical and horizontal movements.

Fuel consumption in such a furnace ranges typically in tens of megawatts. As the furnaces operates throughout the year, the heating process optimization reducing the fuel consumption, scale formation and rejects as well as pollutant emissions and further improving quality of rolled products is the important task for the producers of furnaces.

There are employed in our workplace two ways of obtaining the sufficient information for heating process optimization by the furnace construction and utilization.

The computer modelling have been applied to solve aero-thermo-mechanical processes. The computational system FLUENT (Fluent Inc., 1998a), (Fluent Inc., 1998b) used in our workplace meets almost all our requirements. It solves, using the finite volume method, temperature, velocity and pressure fields inside the continuous pusher-type furnace. The model of the furnace can include real thermal losses through the furnace walls, temperature dependent properties of combustion gases, turbulent flow as well as radiation among inner furnace walls and charge surfaces. Percentage thermal losses on furnace walls and furnace openings related to heat flux to the billets can be monitored. The rate of radiation heat flux to total heat flux can be compared at furnace walls and billet surfaces. Heat flux and coefficient of heat transfer can be evaluated. A number of two-dimensional transverse, longitudinal horizontal and longitudinal vertical cross-sections of the furnace can be created to monitor x-axis, y-axis and z-axis velocities, velocity magnitude, temperature and total, static and dynamic pressures.

On the other hand, direct measurements of temperatures in continuous furnaces provide reliable data of real processes. A special measuring system has been developed by ŠKODA VÝZKUM to enable applications in continuous furnaces (Honner et al., 1999). Electronics for temperature measurement and sample storage in memory has been equipped by thermal barrier cover of sufficient insulation properties. The cover has been successfully tested in the furnace at 1473 K for 2 hours, causing temperature raise of inside electronics only about 25 K. Temperature in the sample billet and in furnace atmosphere can be measured during the whole heating process because the measuring system moves along with the billet throughout the furnace (Honner & Veselý, 1999).

The mentioned two approaches - modelling and measurement have been combined to develop the optimization system of furnace control, which is now delivered by ŠKODA KLATOVY together with their continuous furnaces (Honner, 1999). The system has been built to set optimal zone temperatures according to economical and technological requirements (Honner & Veselý, 1998) during furnace operation. The main part of the system appears the real time computations of heat transfer to find actual temperature of all slabs in the furnace and to predict its evolution.

The contribution is devoted to the pusher-type furnace of the fine rolling-mill at Hrádek Iron and Steelworks, where the optimization control system is currently set to operation. The aim of the contribution is to demonstrate the current capabilities of the aero-thermo-mechanical process computer modelling and to present the obtained results.

2. GEOMETRY OF THE PUSHER-TYPE FURNACE

The distribution of temperatures, velocities and pressures has been modelled in the interior of the pusher-type furnace. The surface of the considered volume (the internal surface of the furnace) is shown in Fig.1.

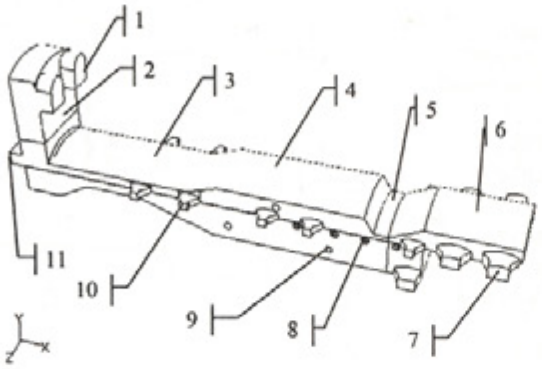

Fig.1: Surface of the considered furnace interior (1... channels to the recuperator, 2... exhaust of combustion gas, 3...front part of the furnace, 4...middle part of the furnace, 5...transition part of the furnace, 6...rear part of the furnace, 7...billet output port, 8...slide shoe support, 9...gas fired burners, 10...manipulation doors, 11...billet entry port)

The origin of the orthogonal coordinate system has been located to the center of billet entry port at the level of upper surface of slide shoes. Dimensions of the volume being modelled in terms of considered axis directions are:

x-axis horizontal, heading from the billet entry port for the rear furnace wall

x_min	=	0 mm	... billet entry port
x_max	=	14005 mm	... rear furnace wall

y-axis vertical, heading from the furnace bottom for the furnace roof

y_min	=	-1020 mm	... the lowest part of the furnace bottom
y_max	=	3040 mm	... the highest part of the combustion gas exhaust roof

z-axis horizontal, heading from the left side wall for the right furnace wall

z_min	=	-1480 mm	... left billet output door
z_max	=	1480 mm	... right billet output door

The overall furnace volume contains 32.940 m^3 of combustion gas atmosphere. The dimensions of the considered billets forming the furnace charge are 90 mm × 90 mm × 1250 mm.

Billets are pushed throughout the preheating and heating zone of the furnace along two water-cooled slide shoes. In the front and partially in the middle part of the furnace the slide shoes are placed on the supporting walls, those divide the region below the billets on 3 parts. These 3 volumes are connected by supporting walls openings at the forepart of the furnace front part. In the rest of the middle and in the transition part of the furnace, the slide shoes are supported by only four water-cooled bearers. There are no supporting walls in this region enabling combustion gasses to circulate around the billets. In the rear part of the furnace billets move directly along the hearth.

Fig.2 shows the interior of the furnace - furnace bottom in the front, middle and transition part, supporting walls, slide shoes and their water-cooled support bearers. There are also billet entry port, billet output ports and rear and side wall burners visible. The billets and all manipulation doors are added to the Fig.3. Fig.4 shows the same except the excluded charge and included furnace walls bellow the level of charge.

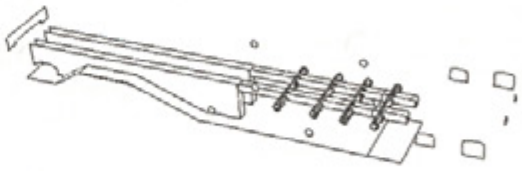

Fig.2: Furnace interior - A

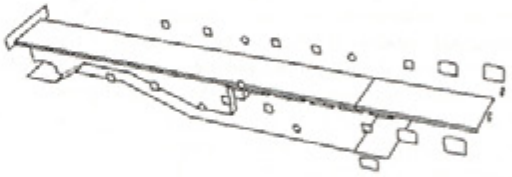

Fig.3: Furnace interior - B

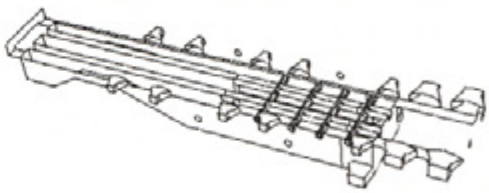

Fig.4: Furnace interior - C

The billets entry port is 1900 mm wide and 360 mm high. The billets output ports have two dimensions: the smaller one of 450 mm wide, max. height 320 mm, semi-diameter of vaulting 850 mm and larger one of 500 mm wide, max. height 400 mm and semi-diameter of vaulting 900 mm.

There are 9 burners situated in side and rear furnace walls. The burner nozzle diameter is 200 mm. Location of all the burners is shown in Fig.5. The burners in side furnace walls are usually placed as a couple - the first burner above the billets and the second on the opposite wall bellow the billets - producing circular stream of combustion gases. The following couple of the burners produces circular stream of the opposite direction

causes the formation of swirls producing a large turbulence in the flow. Two burners are also located at the rear furnace wall symetrically to the side walls.

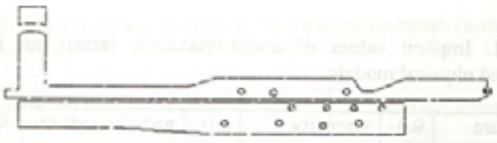

(a) all burners

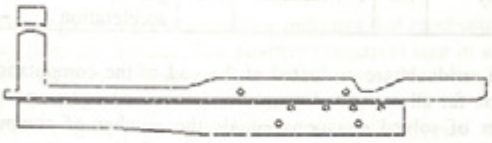

(b) burners at the left side furnace wall

(c) burners at the right side furnace wall

Fig.5: Burners locations

The combustion gas stream generally flows from the burners to the front part of the furnace and through the exhaust to the recuperator.

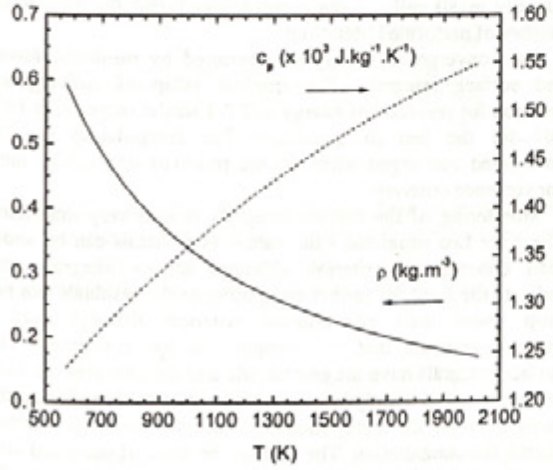

Fig.6: Temperature dependence of mass density and specific thermal capacity of the combustion gas

3. THERMOPHYSICAL PROPERTIES OF THE COMBUSTION GAS

The combustion gas comes from the natural gas combustion with the excess of air 1.1 . Temperature dependence of mass density ρ (kg.m^{-3}) and specific heat capacity c_p (J.kg^{-1}.K^{-1}) is shown in Fig.6. Thermal conductivity k (W.m^{-1}.K^{-1}) and dynamic viscosity μ (N.s.m^{-2}) is shown similarly in Fig.7.

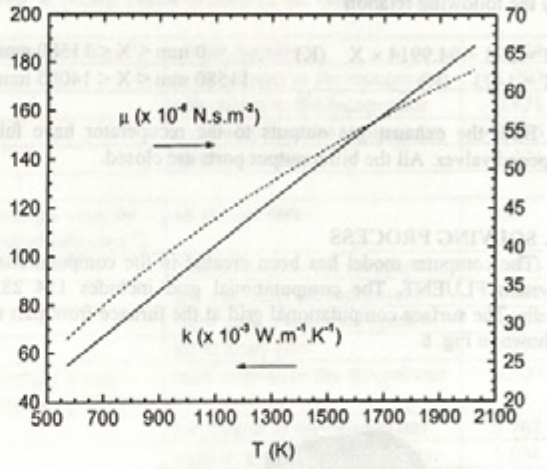

Fig.7: Temperature dependence of thermal conductivity and dynamic viscosity of the combustion gas

4. BOUNDARY CONDITIONS

Steady state solution of the aero-thermo-mechanical processes in the pusher-type furnace is presented on the example of maximum (full) performance of all the gas fired burners. The following list of boundary conditions has been considered on all the internal furnace surfaces:

billets	- prescribed distribution of surface temperature - emissivity ε=0.8
water cooled slide shoe and its support	- prescribed loss heat flux 3500 W.m^{-2} - emissivity ε=0.8
furnace walls, roof and bottom	- prescribed loss heat flux 800 W.m^{-2} - emissivity ε=0.85
manipulation doors and all billet output ports	- prescribed loss heat flux 3000 W.m^{-2} - emissivity ε=0.8
support walls	- prescribed loss heat flux 50 W.m^{-2} - emissivity ε=0.85
partition wall in the combustion gas exhaust	- prescribed loss heat flux 0 W.m^{-2} - emissivity ε=0.8
burners	- combustion gas temperature at nozzle 1923 K - combustion gas velocity at nozzle 60 m.s^{-1} - 10 % input turbulence - characteristic length of turbulence 200 mm - internal emissivity ε=1

exhaust gas	-	free exhaust without overpressure
output to the	-	backflow temperature 1170 K
recuperator	-	internal emissivity ε=1
billet entry	-	free exhaust without overpressure
port	-	backflow temperature 373 K
	-	internal emissivity ε=1

The surface temperature of the billets has been approximated by the following relation

$T = 373 + 94.9914 \times X$ (K)	0 mm < X < 11580 mm
$T = 1473$ (K)	11580 mm < X < 14005 mm

Both the exhaust gas outputs to the recuperator have full opened valves. All the billet output ports are closed.

5. SOLVING PROCESS

The computer model has been created in the computational system FLUENT. The computational grid includes 154 285 cells. The surface computational grid at the furnace front part is shown in Fig. 8.

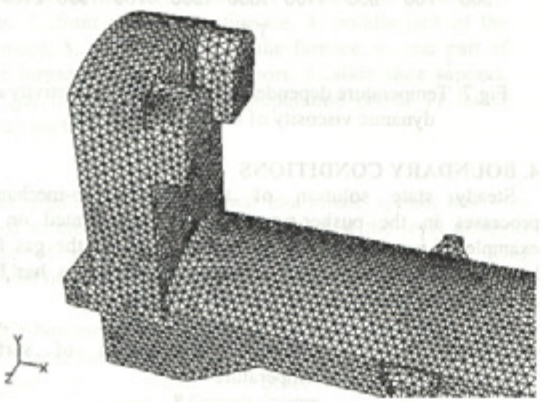

Fig. 8: Surface computational grid

The computer model comprises:

steady state solution
k-ε model of the turbulent flow
heat transfer
the maximum (full) performance of all the gas fired burners
P-1 model of the radiation
- absorption coefficient of combustion gas 0.5 m^{-1}
- scattering coefficient of combustion gas 0 m^{-1}

gravity coefficient – g_y = - 9.80665 $m.s^{-2}$

The backflow temperature in the billet entry port is fixed to 373 K, while the backflow temperature in the combustion gas output to the recuperator has been continuously set during the computation to the average value of the temperature in both outputs to the recuperator.

As the equation system of the mathematical model is nonlinear, it is necessary to control the change of the quantities between the two following computational iterations. It is done by so called under-relaxation. In the most simple form, the new value of the quantity ϕ_P in the cell P is dependent on the old value $\phi_{P,old}$, the computed change of the quantity $\Delta\phi_P$ and the under-relaxation factor α by the equation

$$\phi_P = \phi_{P,old} + \alpha\Delta\phi_P \quad (1)$$

Tab. 1: Implicit values of under-relaxation factors for the included physical models

pressure	0.3	viscosity	1.0	turb.dissipation energy	0.8
momentum	0.7	temperature	1.0	turb. kinetic energy	0.8
density	1.0	P-1 radiation	0.8	gravity acceleration	1.0

The residuals are evaluated at the end of the computational iteration for all computed quantities (all solved equations - the number of solved equations equals the number of computed quantities). The residuals are stored and they witness the convergence history. The residual of the quantity ϕ in the cell P express unbalance in the equation for the quantity ϕ_P in this cell

$$a_P\phi_P = \sum_{neighbour\_cells} a_{nc}\phi_{nc} + b \quad (2)$$

where a_P, a_{nc}, and b are the coefficients evaluated from the thermophysical properties of the fluid and boundary conditions of the model, the sum is over all the neighbour cells. The residual of the quantity ϕ given by the FLUENT is then the sum of the residuals in all cells of the computational grid divided by the sum of LHS of the equation (2)

$$R^{\phi} = \frac{\sum_{all\_cells\_P} \left| \sum_{neighbour\_cells} \left(a_{nc}\phi_{nc}\right) + b - a_P\phi_P \right|}{\sum_{all\_cells\_P} \left| a_P\phi_P \right|} \quad (3)$$

The residual of the quantity ϕ express average error of the quantity in all cells of the computational grid for the certain number of performed iterations.

The convergence history is monitored by residuals, forces and surface integrals. The implicit setup of convergence criterion for residuals of energy and P-1 model radiation is 10^{-6}, 10^{-3} for the rest of quantities. The computation can be considered converged when all the residuals drop under their convergence criterion.

Monitoring of the surface integrals is also very important. There are two situations - the values of residuals can be under their convergence criterion although surface integrals may indicate the need for further computing or the residuals can not drop under their convergence criterion although surface integrals indicate that the computation has converged. The surface integrals have the crucial role and the convergence have to be monitored mainly by them. Mass and total heat fluxes (the sums over all the outer model surfaces) have been watched during the computation. The smaller the sums of mass and total heat fluxes for all the outer surfaces are, the more converged the computation is.

First, the only turbulent flow of combustion gas without thermal and radiation processes has been computed. The computation has converged after 229 iterations with implicit

values of under-relaxation factors, see Tab. 1. Tab. 2 shows mass flux and average x-axis velocity in the billet entry port and outputs to the recuperator. The values in Tab. 2 are presented for the comparison with the simulation where thermal and radiation processes are involved.

Tab. 2: Flow characteristics at the furnaces openings (turbulent flow only)

quantity	mass flux ($kg.s^{-1}$)	average x-axis velocity ($m.s^{-1}$)
outputs to the recuperator	- 1.804	8.91
billet entry port	- 1.169	-10.67

The negative sign in mass flux indicates that combustion gas flows from the furnace. The positive (negative) sign in average x-axis velocity indicate that combustion gas flows heading x-axis (opposite direction to the x-axis).

The following simulation comprises all physical models including thermal and radiation processes. The first 10 iterations only the turbulent flow has been switched on, the next 10 iterations energy equation has been switched on and after that the radiation equation has been included. All the under-relaxation factors must have their implicit values –increase of them leads to the divergence of the computation. The computation has converged after 4198 iterations with all the residuals under their convergence limits. As well the computation has converged from the point of mass and total heat fluxes as can be seen further.

Tab. 3 shows mass and total heat fluxes for all the furnace surfaces and openings after certain number of iterations.

Tab. 3: Gradual increasing of the computation accuracy

number of iterations	mass flux for all the furnace openings ($kg.s^{-1}$)	total heat flux for all the furnace surfaces and openings (W)
30	$-1{,}94 \times 10^{-2}$	5 228 382
100	$-1{,}49 \times 10^{-4}$	4 236 479
200	$-1{,}30 \times 10^{-4}$	3 164 677
534	$-1{,}33 \times 10^{-5}$	2 561 167
817	$-2{,}69 \times 10^{-5}$	2 156 058
1932	$-8{,}06 \times 10^{-6}$	803 357
2707	$-6{,}88 \times 10^{-6}$	301 969
4198	$-1{,}71 \times 10^{-5}$	34 281

The total mass flux from all the gas fired burners is 2.974 $kg.s^{-1}$, the total heat flux from all the gas fired burners is 6 908 205 W. The values in the Tab. 3 illustrate very good convergence in velocity distribution, the relative error is

$$\frac{\left|-1.71\times10^{-5}\right|}{2.974}\times 100 \approx 6\times10^{-4}\,\% \qquad (4)$$

Good convergence has been also achieved in temperature distribution, the relative error is

$$\frac{\left|34281\right|}{6908205}\times 100 \approx 0.5\,\% \qquad (5)$$

6. RESULTS – GLOBAL CHARACTERISTICS

Tab. 4 represents global characteristics of the velocity field and Tab. 5 of the thermal field in the simulated pusher-type furnace. The negative sign shows outflow of mass/heat from the furnace, the positive sign shows inflow of mass/heat to the furnace.

Tab. 4: Global characteristics of the velocity field

mass flux ($kg.s^{-1}$)	all the burners	2.974
	both outputs to the recuperator	- 1.703
	left output to the recuperator	- 0.928
	right output to the recuperator	- 0.775
	billet entry port	- 1.271
average velocity magnitude ($m.s^{-1}$)	all the burners	60
	both outputs to the recuperator	5.603
	left output to the recuperator	6.020
	right output to the recuperator	5.188
	billet entry port	7.677
average x-axis velocity ($m.s^{-1}$)	both outputs to the recuperator	5.500
	left output to the recuperator	5.962
	right output to the recuperator	5.038
	billet entry port	- 7.513

Tab. 5: Global characteristics of the temperature field

heat flux from the burners (W)	total heat flux	6 908 205
	radiation heat flux	244 516
heat flux to the all furnace openings (W)	total heat flux	- 3 287 315
	radiation heat flux	22 278
heat flux to the all furnace walls and charge surfaces (W)	total heat flux	- 3 586 608
	radiation heat flux	- 3 112 949
heat flux to the charge surfaces (W)	total heat flux	- 3 468 571
	radiation heat flux	- 3 209 193
heat flux to the furnace walls (W)	total heat flux	- 118 037
	radiation heat flux	96 244
heat flux to the recuperator (W)	total heat flux	- 1 900 810
	radiation heat flux	5 805
heat flux to the recuperator by the left channel (W)	total heat flux	- 1 024 289
	radiation heat flux	1 380
heat flux to the recuperator by the right channel (W)	total heat flux	- 876 521
	radiation heat flux	4 425
heat flux to the billet entry port (W)	total heat flux	- 1 386 506
	radiation heat flux	16 473

average temperature [K]	all furnace volume	1 405
	billet entry port	1 075
	both outputs to the recuperator	1 163
	left output to the recuperator	1 153
	right output to the recuperator	1 174

6.1. Mass flux comparison

Taking the mass flux that inflows to the furnace from all gas fired burners as 100%, 42.7% of mass flux outflows through the billet entry port and the rest 57.3% outflows to the recuperator. Considering the mass flux outgoing to the recuperator as 100%, 54.5% of mass flux goes by the left channel and 45.5% by the right channel to the recuperator.

The differences between the output combustion gas velocities in Tab. 2 and Tab. 4 are due to large volume expansion of the combustion gas. Including the thermal and radiation processes to the simulation, combustion gas inputs the furnace with the temperature of 1923 K (low density) but outputs the furnace with the lower temperature (higher density). Therefore, taking the constant combustion gas velocity at the nozzle of the burner, the exhaust gas needs lower output velocity in the case including thermal and radiation processes.

6.2. Heat flux comparison

Taking the total heat flux from the gas fired burners to the furnace as 100%, 50.2% goes to the charge surfaces, 1.7% goes to the furnace walls and 47.6% goes by the furnace openings out of the furnace (20.1% goes through the billet entry port and 27.5% through the outputs to the recuperator), the rest 0.5% is the simulation error.

Considering the total heat flux to the all furnace walls and charge surfaces as 100%, 96.7% goes to the charge surfaces, the rest 3.3% to the furnace walls.

Taking the heat flux to the recuperator as 100%, left combustion gas channel include 53.9% and the right combustion gas channel 46.1% of the heat flux to the recuperator.

All the furnace and charge walls take 87% of the absorbed total heat flux by the radiation heat flux. Radiation heat flux to the charge surface is made by 92.5% of the total heat flux to the charge surface. The furnace walls remove the heat from the furnace (total heat flux points out the furnace), but radiation heat flux from the furnace walls supplies the heat to the furnace (radiation heat flux points to the furnace). The reason is that average charge surface temperature is lower than the furnace wall temperature.

The space distribution of the temperature, x-, y- and z-axis velocity, velocity magnitude, velocity vector, static, dynamic and total pressure is conveniently reproduced by the two-dimensional transverse, longitudinal horizontal and longitudinal vertical cross-sections of the furnace. The total number of 66 furnace sections have been created to monitor the three-dimensional distribution of the quantities. Fig. 9 shows the transverse section leading through the fifth furnace side burner at the distance 9155 mm from the billet entry port.

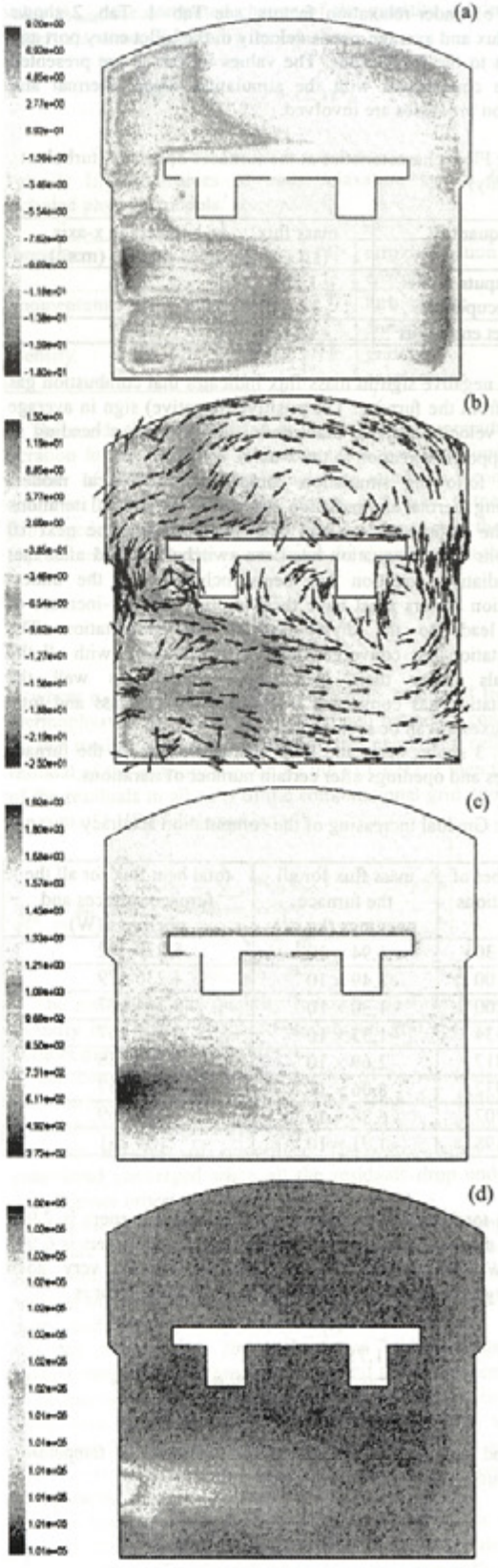

Fig. 9: Distribution of the quantities in the X(21) furnace section - (a) x-axis velocity v_x ($m.s^{-1}$), (b) x-axis velocity v_x ($m.s^{-1}$) + velocity vectors v_{yz}, (c) temperature T (K), (d) total pressure p (Pa)

Fig. 10 shows the temperature T_g (K) and velocity magnitude $|v|_g$ ($m.s^{-1}$) of the combustion gas 150 mm above the upper charge surface along the x-axis direction (only the z = 0 mm line).

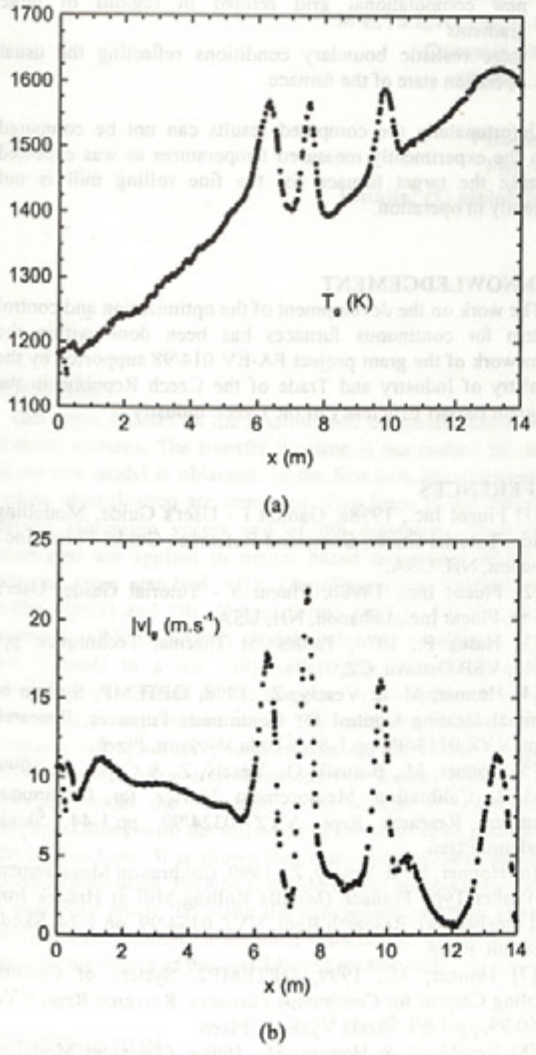

Fig. 10: Distribution of the (a) temperature, (b) velocity magnitude, 150 mm above the upper charge surface along the x-axis (only z = 0 mm line)

The radiation heat flux to the charge surfaces comprises 92.5% of the total heat flux to the charge surface. Fig. 11 shows the total q''_t ($W.m^{-2}$) and radiation q''_r ($W.m^{-2}$) heat fluxes to the upper charge surface along the x-axis direction. The radiation heat flux is - 1.2×10^5 $W.m^{-2}$ at the rear furnace wall. Moving from the rear furnace wal to the transition - rear furnace part interface, the radiation heat flux decreases to the value - 4×10^4 $W.m^{-2}$. Moving from the transition - rear furnace part to the front - middle furnace part interface, the radiation heat flux increases to the value - 1.83×10^5 $W.m^{-2}$. Moving further to the billet entry port, the radiation heat flux decreases to the value - 9×10^4 $W.m^{-2}$.

The convective heat flux q''_c ($W.m^{-2}$) to the upper charge surface has been evaluated from the values of total and radiation heat fluxes, see Fig. 12. The coefficient of heat transfer h ($W.m^{-2}.K^{-1}$) has been computed from the convective heat flux to the upper charge surface and the difference between the combustion gas temperature 150 mm above the upper charge surface (only z = 0 mm line parallel to x-axis) and charge surface temperature (only z = 0 mm line parallel to x-axis), see also Fig. 12.

The value of the heat transfer coefficient is around 20 $W.m^{-2}.K^{-1}$ in the front part of the furnace where are no burners. In the middle furnace part, the heat transfer coefficient follows the pattern of combustion gas velocity - the direct impact of combustion gas from the burners (Fig. 10), the values are generally about 20 to 60 $W.m^{-2}.K^{-1}$ but the peaks reach 100 $W.m^{-2}.K^{-1}$. In the rear furnace part, the combustion gas flow above the charge surface is directly influenced by the two burners at the rear furnace wall and that the heat transfer coefficient increases up to 100 $W.m^{-2}.K^{-1}$.

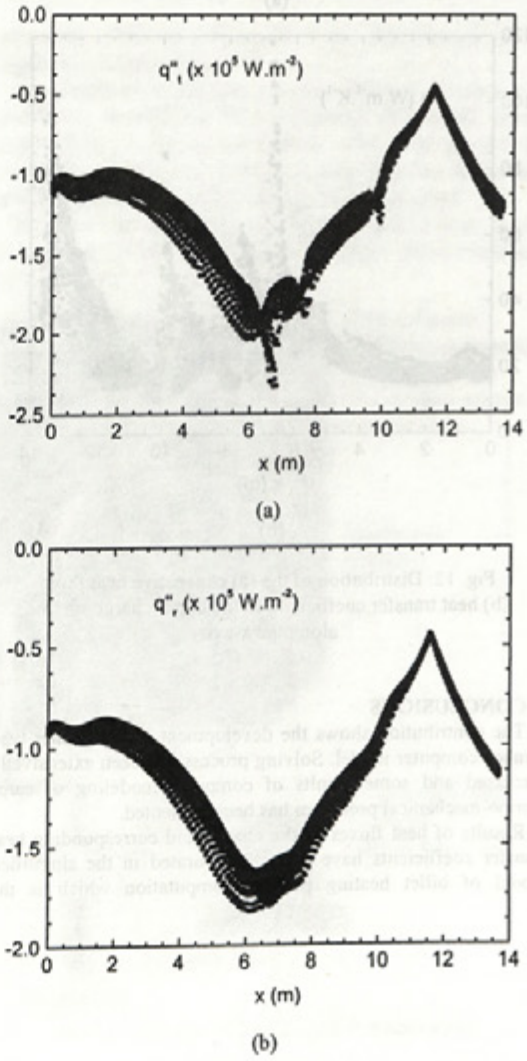

Fig. 11: Distribution of the (a) total, (b) radiation heat fluxes, to the upper charge surface along the x-axis

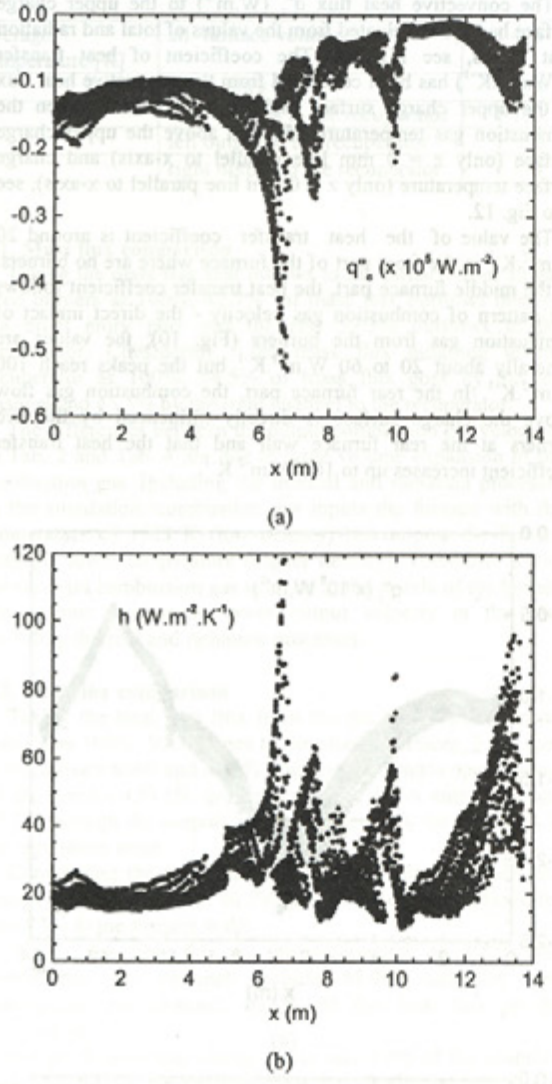

Fig. 12: Distribution of the (a) convective heat flux, (b) heat transfer coefficient, to the upper charge surface along the x-axis

7. CONCLUSIONS

The contribution shows the development of the pusher-type furnace computer model. Solving process has been extensivelly discussed and some results of computer modeling of earo-thermo-mechanical processes has been presented.

Results of heat fluxes to the charge and corresponding heat transfer coefficients have been incorporated in the simplified model of billet heating process computation which is the important part of the real time furnace optimal control system.

The presented model is beeing currently improved to incorporate:

- real charge motion throughout the furnace and computation of temperatures in heated billets
- new computational grid refined in regions of large gradients
- more realistic boundary conditions reflecting the usual operation state of the furnace

Unfortunatelly the computed results can not be compared with the experimently measured temperatures as was expected because the target furnace for the fine rolling mill is not currently in operation.

ACKNOWLEDGEMENT

The work on the development of the optimization and control system for continuous furnaces has been done within the framework of the grant project FA-EV 014/98 supported by the Ministry of Industry and Trade of the Czech Republic in the program Export Efficiency of the Czech Industry.

REFERENCES

[1] Fluent Inc., 1998a, Gambit I - User's Guide, Modelling Guide, Tutorial Guide, Command Reference Guide, Fluent Inc., Lebanon, NH, USA,

[2] Fluent Inc., 1998b, Fluent 5 - Tutorial Guide, User's Guide, Fluent Inc., Lebanon, NH, USA,

[3] Hašek P., 1974, Tables for Thermal Techniques, pp. 1-245, VŠB Ostrava, CZ,

[4] Honner, M. & Veselý, Z., 1998, OPTEMP, System of Optimal Heating Control for Continuous Furnaces, Research Rept. VYZ 0213/98, pp.1-81, Škoda Výzkum, Plzeň.

[5] Honner, M., Borusík, O., Veselý, Z. & Čejka, F., 1999, KALIB, Calibration Measurement Device for Continuous Furnaces, Research Rept. VYZ 0324/99, pp.1-44, Škoda Výzkum, Plzeň.

[6] Honner, M. & Veselý, Z., 1999, Calibration Measurement of Pusher-Type Furnace (Middle Rolling-Mill at Hrádek Iron and Steelworks), Research Rept. VYZ 0354/99, pp.1-24, Škoda Výzkum, Plzeň.

[7] Honner, M., 1999, OPTEMP2, System of Optimal Heating Control for Continuous Furnaces, Research Rept. VYZ 0360/99, pp.1-69, Škoda Výzkum, Plzeň.

[8] Veselý, Z. & Honner, M., 1998a, Computer Model of Thermomechanical Process in Pusher-Type Furnace, Part.1-Model Development, Research Rept. VYZ 0217/98, pp.1-61, Škoda Výzkum, Plzeň.

[9] Veselý, Z. & Honner, M., 1998b, Computer Model of Thermomechanical Process in Pusher-Type Furnace, Part.2-Alt. MAX Results, Research Rept. VYZ 0273/98, pp.1-50, Škoda Výzkum, Plzeň.